IOP Conference Series: Materials Science and Engineering

Corrosion inhibitory properties of $La_{0.5}Ca_{0.5}MnO_3$-gold nanoparticles in 1 M HCl

IOP Conf. Series: Materials Science and Engineering **509** (2019) 012039 doi:10.1088/1757-899X/509/1/012039

Corrosion inhibitory properties of $La_{0.5}Ca_{0.5}MnO_3$-gold nanoparticles in 1 M HCl

Abiola Edobor-Osoh[1,3,a,*], Benedict Iserom Ita[2,b], Kolawole Oluseyi Ajanaku[1,c], P. de la Presa[3,d], Cyril O. Ehi-Eromosele[1,e], Miguel Angel Cobos Fernández[3,f], Bamidele Durodola[1,g]

[1] Department of Chemistry, Covenant University, Ota, Ogun State, Nigeria.
[2] Department of Pure and Applied Chemistry, University of Calabar, Cross River State, Nigeria
[3] Applied Magnetism Institute, UCM-ADIF-CSIC, 28230, Las Rozas, Spain.
* Author: [a,*] abiola.edobor@covenantuniversity.edu.ng; [b] iserom2001@yahoo.com;
[c] kola.ajanaku@covenantuniversity.edu.ng; [d] pm.presa@pdi.ucm.es;
[e] cyril.ehi-eromosele@covenantuniversity.edu.ng; [f] micobos@ucm.es;
[g] bamidele.durodola@covenantuniversity.edu.ng

Abstract. The morphological, magnetic, transport and corrosion inhibitory property of $La_{0.5}Ca_{0.5}MnO_3$-AuNPs prepared by sol gel method was determined. The structural property determined by XRD indicated that the unusual broadening of the Bragg's reflection despite the elevated sintering temperature was as a result of the inhibition of the grain growth by the gold nanoparticles (Au-NPs). The morphological property of the sample as determined by SEM and TEM show heterogeneously sized and shaped nanoparticles of an average particle size of 40 nm. The magnetic measurements of $La_{0.5}Ca_{0.5}MnO_3$-AuNPs showed that the sample undergoes a paramagnetic – ferromagnetic phase transition with T_C = 250K and T_B = 150K. Two metal-insulator transitions were observed at T_1 and T_2. The resistivity of the sample was observed to reduce as temperature increased to 300 K. The gravimetric method was used to determine the corrosion inhibitory properties with 1.0 M HCl using different concentration of $La_{05}Ca_{0.5}MnO_3$-AuNPs. The anti-corrosion study was carried out for 21 days and was observed to reduce as concentration of $La_{0.5}Ca_{0.5}MnO_3$-AuNPs increased, but corrosion rate increased as the exposure time increased. The inhibitory property of the sample increased as the concentration of the sample increased. The reaction best fitted the Langmuir isotherm, indicating a monolayer of $La_{0.5}Ca_{0.5}MnO_3$-AuNPs inhibiting the corrosion of the mild steel.

1. Introduction

Corrosion occurs when a material (metal) oxidizes back to its stable state; the change in its chemical state is due to the interaction of the material (metal) with its environment [1]. Corrosion has posed a great threat to the economic value of various countries [2]. In 2014, China lost a total amount of 921.22 billion RMB to corrosion alone [3]. Mild steel is one of the commonly used alloys in the industries due to its malleability and reduced purchasing cost. The failure of engineered mild steel in the industries has become a major contributing factor to the total rate of loss due to corrosion of metal in the world. The use of mild steel in various industries cannot be overemphasized as mild steel takes over 50% of all the metals employed in manufacturing the equipment utilized in processing industries [4]. The cost of maintenance of instruments such as reactors, mixing bowls etc. has become very unbearable for many

industrialists. The use of corrosion inhibitors has been the best solution to the challenge of corrosion. The use of organic inhibitors has taken the fore-front in hindering the anodic/cathodic reactions of metals with its alkaline/acidic environment. Although organic inhibitors are very effective, however, the toxicity of the inhibitors has been a trending topic in the corrosion inhibition study as they do not meet the environment protection standards. Nano-inorganic inhibitors are compounds of inorganic nature with particulate size of 10^{-9} m (nm). The advantages of inorganic nanoparticles as inhibitors have been situated by a number of researchers [4-6].

Manganites are perovskites with the transition element manganese (Mn) as a constituent in the compound; and it has the general notation $REMnO_3$. The structure of the oxide of composition $(RE_{1-x}AE_x)MnO_3$ (doped manganite) is similar to that of the REO_3 structure (the parent manganite), where RE denotes a trivalent rare earth ions (Lanthanides: lanthanum, neodymium, praseodymium etc.) and AE is a divalent alkaline ion (calcium, strontium or barium) (used in doping the parent manganite), and they are generally called mixed valence manganites [7]. Mixed valence manganites generally possess unique intrinsic properties that determine their application in industries. Such properties include magneto-caloric effect, magneto-resistance, transport properties etc. Although mixed-valent manganites have been studied for almost 50 years, the quality of the intrinsic properties of the manganites has induced the popularity of investigations by a sizable fraction of the condensed matter community. Manganites based perovskites are well known for providing a thrust for the beginning of numerous technological applications that are based on magneto-electric, magneto-resistance, magneto-capacitive and magneto-caloric effects [8-15]. Although manganites have so much potential as described above, only a few researches has been undertaken on the prospect of manganites in combating corrosion. We therefore investigate the structural, morphological, magnetic and corrosion inhibitive properties of the nanocomposite, $(La_{0.5}Ca_{0.5}MnO_3)_{1-x}/AuNP_x$.

2. Materials and Methods

2.1. Synthesis and Characterization of LCMO1100 and LCMO-AuNP 1100

LCMO-AuNP1100 nanocomposite was synthesized by use of a modified sol gel method ([16]. Solutions of precursors La_2O_3, $CaCO_3$ and $MnCO_3$ with 99.9% were stoichiometrically mixed at a mole ratio 3.3:6.7:10 of La, Ca and Mn. The precursors were dissolved in nitric acid. Citric acid and ethylene glycol were added, periodically. The solution was heated on a hot plate while stirring at 90ºC until a xerogel was formed.

Gold nanoparticles were used as prepared by Lee *et al.* [17]. Gold nanoparticles were added to the xerogel and heated continuously until a fluffy mass of LCMO-AuNP1100 was formed. The dark brown powder was milled using a mortar and pestle until all samples were uniformly sized. The sample was annealed at 600ºC for 24 hours to remove all organic compounds. Pure crystalline particles obtained were pelletized using Mega-Berux-Vizcaya 15 tonnes at 350 kg/cm^2. 10 mg of sample was placed in a 13 mm die cast (Specac PT. No. 3000) and annealed at 1100ºC for 24 hours. The samples were kept in the furnace until it slowly cooled at room temperature. X-ray diffraction pattern of the bare and doped manganite was obtained using PANalytical X'pert Pro MPD diffractometer Cu-Kα radiation source at room temperature. Scanning Electron Microscope JEOL JSM 6400 was used in determining the surface morphology of the gold doped manganites while EDS was utilized in determining the nominal composition of the bare samples. The nominal composition of the samples was determined using a JEOL Superprobe JXA-8900M. The TEM images were determined using JEOL JEM 2100 electron microscope. The M(T) was determined by using Quantum Design SQUID (MPMS 5 Quantum Design cryo-magnet 5T; cryostat 2–400 K. The Zero Field Cooling (ZFC) (measured after cooling in zero field) and Field Cooling (FC) temperature dependent curves were measured at 5 – 300 K under an external cooling field of 1000 Oe [16].

The proposed equation of reaction based on the precursors used is as described below:

$$\frac{1}{4}La_2O_3 + \frac{1}{2}CaCO_3 + MnCO_3 + AuNP \rightarrow La_{0.5}Ca_{0.5}MnO_3 - AuNP + \delta CO_2 \uparrow$$

2.2. Corrosion Analysis of LCMO-AuNP 1100

Mild steel sheets of composition (wt%) Mn (0.90), C (0.12), S (0.066), P (0.050), Si (0.10) and Fe (98.764) were used for the study. The mild steel was cut into coupons 3×2×0.1 cm dimension and abraded with a series of emery paper of different grades (No. 60, 120, 220 and 600). Each coupon was washed using distilled water, degreased and dried by acetone. The coupons were weighed using (RADWAG AS310/C/2, Maximum 310 g and density = 0.1 mg). All the coupons were kept in a desiccator, prior to use. The concentrations of the inhibitor were 0.02 g, 0.05 g and 0.1 g dissolved in 1.0 M HCl prepared by dilution of analytical grade 37 % HCl with distilled water.

2.3. Weight Loss Measurement

Gravimetric measurements are carried out in a 250 mL beaker and a thermostatic water bath at 25ºC is used throughout the period of the study. 150 mL of the aggressive solution was used for the study. The time for immersion into the solution for the weight loss (g) study was 21 days. Dataset were acquired every 3 days (72 hours), the specimens are removed from the beaker and the reaction is stopped by using a washing agent and dried in acetone. The coupons were then weighed to determine the effect of inhibitor on the corrosion reaction [18]. The dataset showed that weight loss decreased as the concentration of LCMOAuNP1100 increased from 0 – 0.1 g.

The corrosion rate (C_R) was determined by using the equation,

$$C_R = 87.6 \left(\frac{W_L}{DAT}\right)$$

W_L = Weight loss in mg
D = Metal Density (7.85 g/cm^3)
A = Area of sample in cm^2
T = Time of exposure of metal exposure in hours

The corrosion rate in mm/yr (millimeter per year) was converted to mpy (mils penetration per year) by a conversion factor of 0.0254 mm/yr = 1 mpy.

The inhibition efficiency was calculated using the equation,

$$I.E\ \% = \frac{\Delta M_0 - \Delta M_{inh}}{\Delta M_0} \text{ x } 100$$

Where, ΔM_0 is the difference between the initial weight and final weight after coupon has been immersed into 1 M HCl solution

ΔM_{inh} is the difference between the initial weight and final weight after the coupon has been immersed into 1 M HCl and different concentrations of inhibitors.

3. 3. Result and Discussion

3.1. Structural Analysis of the Manganites

The bare and doped manganite exhibited the same characteristics peaks of an orthorhombic perovskite. The relative peak intensity of the diffraction peaks increases as gold nanoparticles was doped, showing better crystallinity.

The mean crystallite size <D> was calculated from the Scherer's formula [19, 20] to be approximately, 40.126 nm.

$$D = \frac{0.9\lambda}{\beta_{FWHM} Cos\ \theta}$$

Where, 0.9 is a constant
Λ = 0.154 nm
β_{FWHM} = Full width at half maximum of the X-ray reflection in radian
θ = Position of the highest intensity

The manganite does not show the peaks of gold nanoparticles; this may be due to the uniform dispersion of the gold nanoparticle in the composite formed with manganite. However, the crystallite size of manganite increased with doping [21].

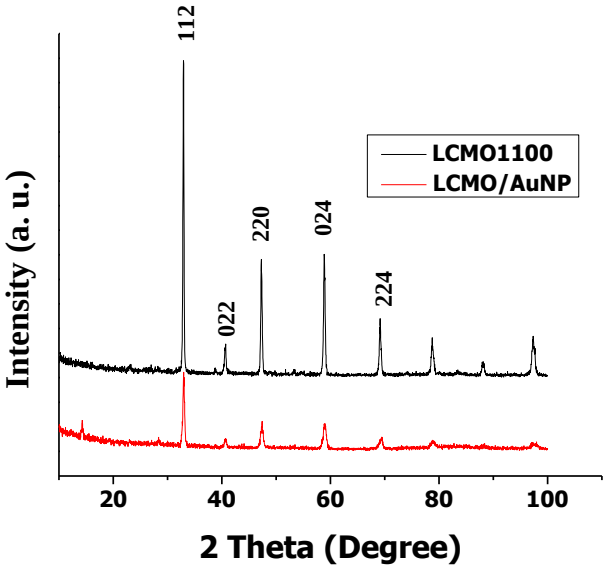

Figure 1. X-ray diffraction pattern of LCMO1100 and LCMO-AuNP 1100 (red line).

3.2. Morphological Properties and Composition of Manganites

The SEM micrograph of LCMO1100 and LCMO-AuNP 1100 are as shown in Fig. 2(a) and (b). The connectivity of the grains increased as the manganite is doped with gold nanoparticles [22]. The average composition of the sample was determined as $La_{0.51}Ca_{0.47}Mn_{1.02}O_3$. The average composition of gold nanoparticles is much lower than the nominal composition as it was observed as $La_{0.57}Ca_{0.60}Mn_{1.04}O_3$-$AuNP_{0.009}$; this might be due to the evaporation of the gold nanoparticles as a result of the high sintering temperature used, while the nominal composition of the bare nanoparticles showed that the sample contained all the components and the decrease/increase in average and nominal composition was due to experimental errors.

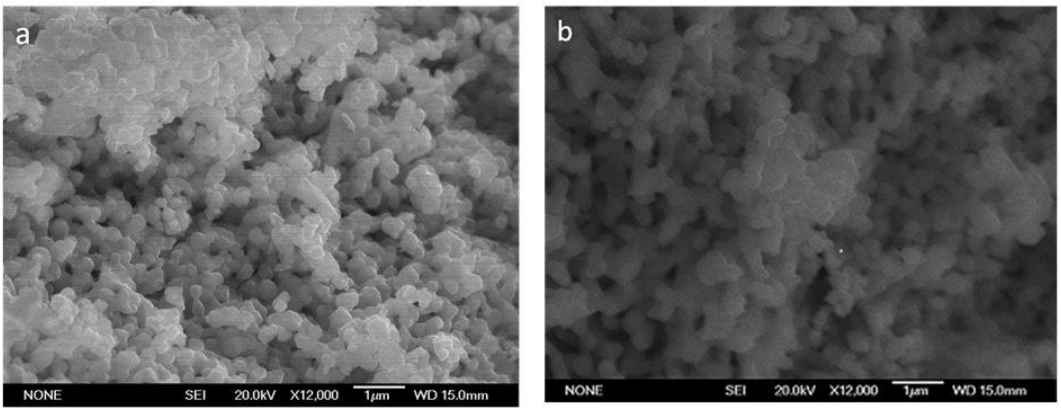

Figure 2. SEM images of (a) LCMO1100 and (b) LCMO-AuNP 1100.

The TEM image (Fig. 3(a) and (b) shows that the particles were heterogeneously sized with the average particles size of 164 nm as determined by Image J. Fig 3 (a) shows pseudo-cubic shaped

particles of LCMO1100 which shows that the sample is indeed a perovskite sample. In Fig. 3(b) shows that the size and shape of the particles changed as the manganite was doped with gold nanoparticles.

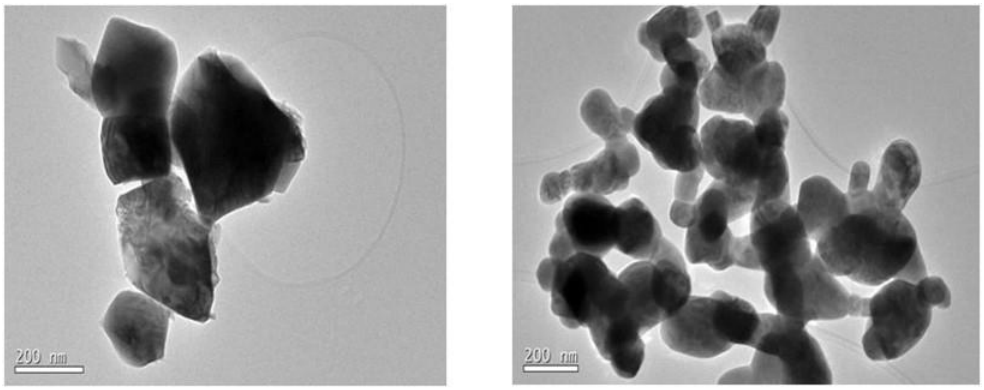

Figure 3. TEM images of (a) LCMO1100 and (b) LCMO-AuNP 1100.

3.3. Magnetic and Transport Properties of LCMO-AuNP 1100

A steady decrease of magnetization was observed from 210 K at 20 emu/g from the ZFC-FC curve described in Fig. 4(a). A sharp reduction of magnetization was observed at 300K, indicating the change in magnetic transition of the sample [23]. The blocking temperature (T_B) was determined from the M(T) curve at 1000 Oe. This describes the temperature at which the system begins to respond to an external applied field as temperature increased indicating the onset of magnetic irreversibility with a spin glass property [24, 25] for LCMO-AuNP 1100 T_B was approximately 150 K [26]. The Curie temperature (T_C) was determined from a plot of dM/dT vs T as 250ºC.

The resistivity study of the material (Fig. 4(b)) is determined by using four probe method temperatures ranging from 5 to 300 K; metal-insulator phase transition is observed for the sample. A cusp curve with two phases was observed the metallic region where resistance increased with rise in temperature, it reaches a peak at the metal-insulator transition temperature (T_{MI}) approximately 125 K and another phase above T_{MI} called the charge ordered insulating region, where resistivity plunges as temperature rises to 300 K [26, 27]. Double peaks have been observed in the electrical transportation curve of various polycrystalline manganite, this may be due to the inter-grain and/or intra-grain resistivity of the sample.

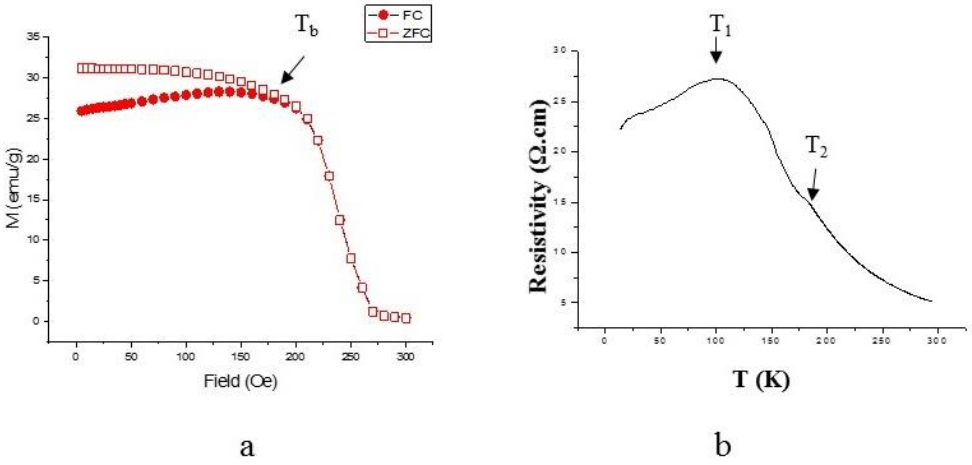

Figure 4. (a) ZFC-FC curves and (b) temperature dependence resistivity for LCMO-AuNP 1100.

3.4. Weight Loss Analysis

Fig 5 (a)-(c) shows the weight loss, corrosion rate (mpy) and inhibition efficiency (I.E. %) determined at concentrations (0.02 g, 0.05 g and 1.0 g) of LCMO-AuNP 1100, respectively. Fig. 5(a) illustrates the changes observed in weight of mild steel due to the aggressive environment 1 M HCl it was immersed in. The weight loss was measured for 21 days. It was observed that weight loss of the coupons reduced as the concentration of the inhibitor increased which might be due to an increased surface coverage and adherence of the inhibitor to the metal. The abrupt decrease in weight loss for all the concentrations indicates that the maximum exposure time for unsurpassed efficiency of the sample was 15 days [28]. Comparison of the blank and the inhibited corrosion study showed that the inhibitor influenced the rate of corrosion of mild steel in 1 M HCl. The study was done at 298 K. Fig. 5(b) confirms that the rate of corrosion of mild steel in 1 M HCl reduces as the concentration of LCMO-AuNP 1100 increases [29, 30]. The comparison of the corrosion rate and weight loss shows an inverse proportion. The corrosion rate of the sample is varied as the exposure time increases from 6 days to 21 days.

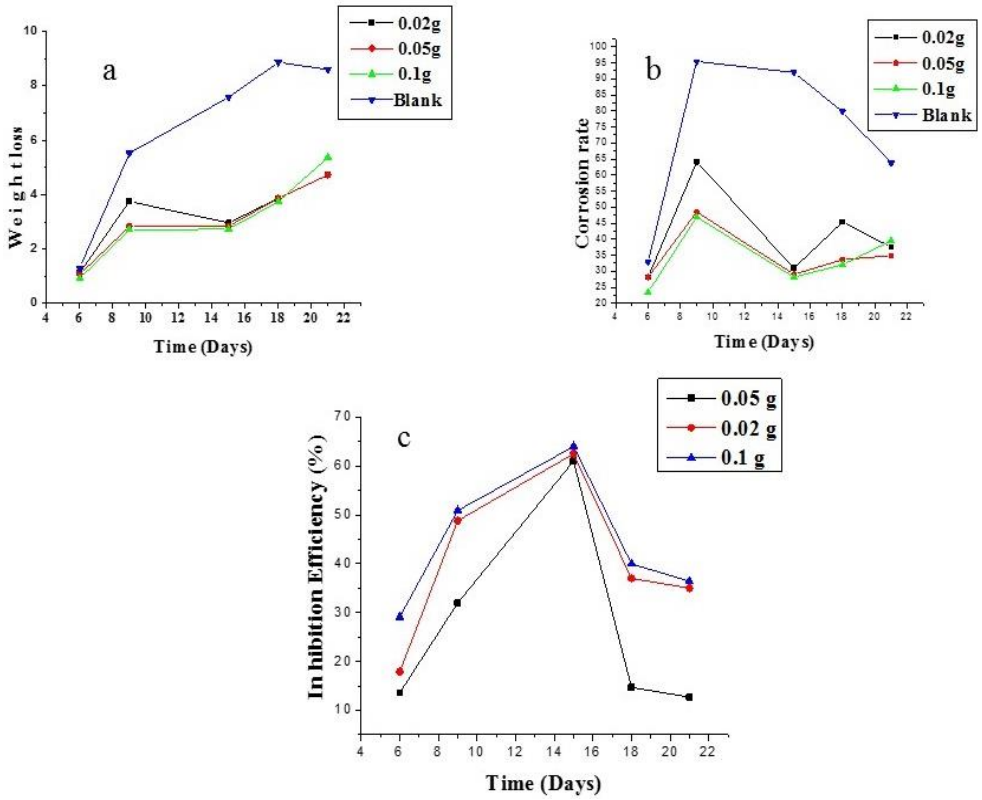

Fig. 5: Graph of (a) weight loss (b) corrosion rate (c) inhibition efficiency against time (days) for variations of concentrations of LCMO-AuNP 1100

3.5. Adsorption Isotherm

The adsorption isotherms (Figs. 6 (a) and (b)) are the Langmuir and Freundlich adsorption isotherms, respectively. They were determined to provide information of the interaction among the adsorbed molecules as well as with their metal or alloy surface [29]. The surface coverage was fitted to a series of different adsorption isotherms including Langmuir isotherm and Freundlich isotherm. The Langmuir adsorption isotherm was observed to be the best adsorption characteristics of LCMO-AuNP 1100. The plotting values of log $\frac{C}{\theta}$ versus log C shows a straight line graph with R^2 = 0.999 while Freundlich isotherm has R^2 = 0.998. The Langmuir isotherm was close to unity, best explaining the relationship between the molecules and the mild steel.

The Langmuir isotherm was determined by the equation:

$$\frac{C}{\theta} = \frac{1}{K_{ads}} + C$$

The Freundlich isotherm was determined by the equation:

$$\log\theta = \log K_{ads} + n\log C$$

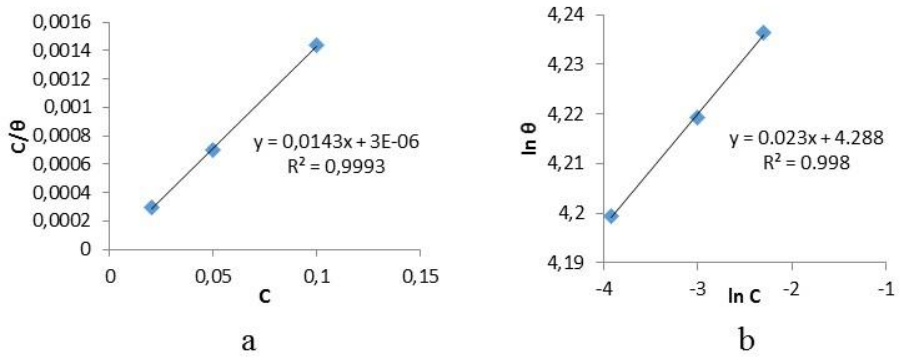

Fig. 6: (a) Langmuir and (b) Freundlich adsorption isotherms of LCMO-AuNP 1100 on the surface of mild steel in 1.0 M HCl.

4. 4. Conclusion

It was noted that the peak intensity of the XRD and the connectivity of the particles increased as gold nanoparticles was doped in the manganite. The resistivity of LCMO-AuNP 1100 shows a metallic-insulating phase transition. The M(T) showed that the sample had a magnetic property as observed from the T_C and T_B. Corrosion inhibition properties of LCMO-AuNP was analysed, showing that the corrosion inhibition of the nanocomposite $(La_{0.5}Ca_{0.5}MnO_3)_{1-x}/Au_x$ increased as concentration increased but inhibition efficiency reduced as the time of exposure increased.

Acknowledgements

We would like to acknowledge Applied Magnetism Institute, Laz Rosaz, Madrid, for granting us the use of their equipment for this research and also Covenant University, Ota, Ogun State, for funding the research.

References

[1] Shaw B A and Kelly R G 2006 What is corrosion? *Electrochem. Soc. Interface* **15** 1 24-7
[2] Rodriguez-Clemente E, Gonzalez-Rodriguez J, Valladarez-Cisneros M, Chacon-Nava J, Flores-De los Ríos J and Rodriguez-Valdez L 2017 Experimental and Theoretical Evaluation of Allicin as Corrosion Inhibitor for Carbon Steel in Sulfuric Acid *Journal of Materials and Environmental Sciences* **8** 11 3817-33
[3] Hou B, Li X, Ma X, Du C, Zhang D, Zheng M, Xu W, Lu D and Ma F 2017 The cost of corrosion in China *Mater. Degrad.* **1** 1 4
[4] Yang F, Li X, Dai Z, Liu T, Zheng W, Zhao H and Wang L 2017 Corrosion Inhibition of Polydopamine Nanoparticles on Mild Steel in Hydrochloric Acid Solution *Int. J. Electrochem. Sci.* **12** 8 7469-80
[5] Atta A M, El-Mahdy G and Al-Lohedan H A 2013 Corrosion inhibition efficiency of modified silver nanoparticles for carbon steel in 1 M HCl *Int. J. Electrochem. Sci.* **8** 4 4873-85
[6] Palanisamy K, Devabharathi V and Sundaram N M 2014 Corrosion Inhibition Studies Of Mild

Steel With Carrier Oil Stabilized Of Iron Oxide Nanoparticles Incorporated Into A Paint *Environ.* **1** 2
[7] Coey J, Viret M and Von Molnar S 1999 Mixed-valence manganites *Adv. Phys.* **48** 2 167-293
[8] Anderson P W and Hasegawa H 1955 Considerations on double exchange *Phys. Rev.* **100** 2 675
[9] Hundley M, Nickel J, Ramesh R and Tokura Y 1998 Science and technology of magnetic oxides. (Warrendale, PA (United States): Materials Research Society)
[10] Scott J 2007 Data storage: Multiferroic memories *Nat. Mater.* **6** 4 256
[11] Phan M-H and Yu S-C 2007 Review of the magnetocaloric effect in manganite materials *J. Magn. Magn. Mater.* **308** 2 325-40
[12] Bibes M and Barthélémy A 2008 Multiferroics: Towards a magnetoelectric memory *Nat. Mater.* **7** 6 425
[13] Wu S, Cybart S A, Yu P, Rossell M, Zhang J, Ramesh R and Dynes R 2010 Reversible electric control of exchange bias in a multiferroic field-effect device *Nat. Mater.* **9** 9 756
[14] Franco V, Blázquez J, Ingale B and Conde A 2012 The magnetocaloric effect and magnetic refrigeration near room temperature: materials and models *Annu. Rev. Mater. Res.* **42**
[15] Sharma G, Tripathi T, Saha J and Patnaik S 2014 Magnetic entropy change and critical exponents in double perovskite Y2NiMnO6 *J. Mag. Mag. Mater.* **368** 318-23
[16] Iniama G, de la Presa P, Alonso J, Multigner M, Ita B, Cortés-Gil R, Ruiz-González M, Hernando A and Gonzalez-Calbet J 2014 Unexpected ferromagnetic ordering enhancement with crystallite size growth observed in La0. 5Ca0. 5MnO3 nanoparticles *J. App. Phys.* **116** 11 113901
[17] Lee J-H, Choi S U, Jang S P and Lee S Y 2012 Production of aqueous spherical gold nanoparticles using conventional ultrasonic bath *Nanoscale Res. Lett.* **7** 1 420
[18] Arockiasamy P, Sheela X, Thenmozhi G, Franco M, Sahayaraj J W and Santhi R J 2014 Evaluation of corrosion inhibition of mild steel in 1 M hydrochloric acid solution by Mollugo cerviana *Int. J. Corros.* **2014**
[19] Scherrer P 1918 Determination of the size and internal structure of colloidal particles using X-rays *Nachr. Ges. Wiss. Göttingen* **2** 98-100
[20] Ehi-Eromosele C O, Olugbuyiro J, Edobor-Osoh A, Adebisi A, Bamgboye O and Ojeifo J 2018 Magneto-Structural and Antimicrobial Properties of Sodium Doped Lanthanum Manganite Magnetic Nanoparticles for Biomedical Applications: Influence of Silica Coating *J. Biomim. Biomater. Biomed. Eng.* **37** 117-27
[21] Gültekin A 2014 Effect of Au nanoparticles doping on the properties of TiO2 thin films *Mater. Sci.* **20** 1 10-4
[22] Phong P, Dai N, Manh D, Khiem N and Phuc N 2014 Magnetic Surface Effects and Magnetoresistance in Manganite-based Composite Nanoparticles *J. Supercon. Nov. Magn.* **27** 4 1049-58
[23] Loudon J and Midgley P 2006 Micromagnetic imaging to determine the nature of the ferromagnetic phase transition in La 0.7 Ca 0.3 MnO 3 *Phys. Rev. Lett.* **96** 2 027214
[24] Lu C, Hu N, Yang M, Xia S, Wang H, Wang J, Xia Z and Liu J-M 2014 High magnetic field phase diagram in electron-doped manganites La 0.4 Ca 0.6 Mn 1− y Cr y O 3 *Sci. Rep.* **4** 4902
[25] Hansen M F and Mørup S 1999 Estimation of blocking temperatures from ZFC/FC curves *J. Mag. Mag. Mater.* **203** 1-3 214-6
[26] Sergeenkov S, Ausloos M, Bougrine H, Rulmont A and Cloots R 1999 Anomalous temperature behavior of the resistivity in lightly doped manganites around a metal-insulator phase transition *J. Exp. Theor. Phys. Lett.* **70** 7 481-7
[27] Khan S and Singh R 2007 Temperature Profile of Resistivity of Manganites *Mod. Phys. Lett. B* **21** 26 1795-805
[28] Song Y, Jiang G, Chen Y, Zhao P and Tian Y 2017 Effects of chloride ions on corrosion of ductile iron and carbon steel in soil environments *Sci. Rep.* **7** 1 6865
[29] Aladesuyi O, Fatile B, Adedapo E, Ogunboyejo A, Ajanaku C, Olanrewaju I, Ajani O and

Ajanaku K 2016 Corrosion inhibitive effect of 2-(1-(2-Oxo-2H-Chromen-3-Yl) ethylidene) hydrazine carboxamide on zinc-aluminum alloy in 1.8 M hydrochloric acid *Int. J. Adv. Res. Chem. Sci.* **3** 2 15-21

[30] Akinsiku A A, Dare E O, Ajanaku K O, Adekoya J A, Alayande S O and Adeyemi A O 2016 Synthesis of silver nanoparticles by plant-mediated green method: optical and biological properties *Journal of Bionanoscience* **10** 3 171-80